Optimal Placement of Baseband Functions for Energy Harvesting Virtual Small Cells

Dagnachew A. Temesgene, Nicola Piovesan, Marco Miozzo, Paolo Dini

CTTC/CERCA, Av. Carl Friedrich Gauss, 7, 08860, Castelldefels, Barcelona, Spain
{dtemesgene, npiovesan, mmiozzo, pdini}@cttc.es

***Abstract*—Flexible functional split in Cloud Radio Access Network (CRAN) greatly overcomes fronthaul capacity and latency challenges. In such architecture, part of the baseband processing is done locally and the remaining is done remotely in the central cloud. On the other hand, Energy Harvesting (EH) technologies are increasingly adopted due to sustainability and economic advantages. Power consumption due to baseband processing has a huge share in the total power consumption breakdown of smaller base stations. Given that such base stations are powered by EH, in addition to QoS constraints, energy availability also conditions the decision on where to place each baseband function in the system. This work focuses on determining the performance bounds of an optimal placement of baseband functional split option in virtualized small cells that are solely powered by EH. The work applies Dynamic Programming (DP), in particular, Shortest Path search is used to determine the optimal functional split option considering traffic requirements and available energy budget.**

***Index Terms*—energy harvesting, virtual base stations, flexible functional split, CRAN, SDN, NFV, dynamic programming**

I. Introduction

Cloud Radio Access Network (CRAN) ensures cloudification of RAN by centralized pooling of the Baseband (BB) processing units [1]. The need for high capacity and very low latency fronthaul is the major challenge behind the full realization of CRAN. To alleviate this problem, flexible functional split between local base station (BS) sites and a central Baseband Unit (BBU) pool is proposed [2]. By executing some baseband processing tasks locally, the tight latency and bandwidth requirement of the fronthaul can be relaxed, while maintaining many of the centralization advantages that CRAN architecture offers. In addition, Heterogeneous CRAN (HCRAN) is proposed as an architecture that includes a presence of High-Power Nodes (HPNs) for control plane functions and coverage [3] to partially alleviate the fronthaul constraint in CRAN. Moreover, Network Function Virtualization (NFV) enables network functions to be executed on general purpose computing hardware and Software Defined Networking (SDN) is a tool to realize the management and control of these network functions [4].

On the other hand, energy sustainability is one of the key pillars for future mobile network design and operation due to environmental concerns and costs. For this reason, Energy Harvesting (EH) technology is increasingly adopted as a means to ensure sustainability for next generation mobile networks [5]. However, EH comes with its own unique challenge mainly due to unreliable energy sources. Hence, in Energy Harvesting Base Stations (EHBSs), it is important to properly manage the harvested energy and to ensure proper energy storage provision to avoid energy outage.

Most of the literature on energy management policy in EHBSs focuses on a HetNet architecture with an intelligent switching on/off scheduling of base stations. The authors in [6] apply a ski-rental framework based online algorithm for optimal switch on/off scheduling of EHBSs. On the other hand, the authors in [7] apply reinforcement learning to optimize the energy usage. A similar problem of energy saving optimization in HetNets is studied in [8], where multi-armed bandit is applied to determine optimal cell expansion bias. The authors in [9] apply Dynamic Programming (DP) to determine the optimal switch on and off policy of a HetNet by considering the traffic variation and energy arrival.

Nevertheless, embedding EH and incorporating flexible functional split options in HCRAN is missing in the literature. The functional splits give insight into considering more operation modes of BSs, in addition to switch on and off. This paper starts filling this gap by investigating the performance bounds of an optimal energy management scheme that incorporates functional split options. The proposed approach is unique by considering more operational modes of virtual small cells as compared to the current literature that focuses only on intelligent switching on and off policies.

The main contributions of the paper are:

- Proposing an HCRAN scenario involving a central BBU pool and local virtualized small cells having capabilities of EH with dynamic placement of functional split options. The scenario relies on NFV for the dynamic movement of baseband processes as virtual network functions between the local virtual small cell sites and the central BBU pool, according to the choice of the functional split option.
- Formulating the energy management of virtual EHBSs and a central BBU pool as an offline optimization problem targeting three functional split options, namely MAC/PHY, UpperPHY/LowerPHY and CRAN, in addition to the switching off;
- Applying a DP algorithm to find the optimal placement of the functional split options considering the traffic demand, energy reserve and forecasted energy arrival. In particular, Shortest Path search is applied for solving the optimization problem;
- Presenting the performance bounds of the optimal place-

ment of functional split options and a comparison against static network configurations. Hence, the numerical results can serve as guidelines for designing online optimization approaches.

The rest of the paper is organized as follows. Section II describes the considered network scenario. Section III introduces the system model. In Section IV, the optimization problem and the optimal algorithm are described. The results are discussed in Section V. Finally, we draw our conclusions in Section VI.

II. Network Scenario

We consider a RAN as a set of clusters of one Macro Base Sation (MBS) with co-located BBU pool and N virtual Small Cells (vSCs). The vSCs provide service to hotspots, whereas mobility and baseline coverage are provided by the MBS. The vSCs are fully powered by EH plus batteries and are endowed with limited computational resource that can be used opportunistically, e.g., when enough energy is available, for part of the baseband signal processing tasks. The MBS with the BBU pool is powered by the electrical grid. The connection between vSCs and MBS is provided by a reconfigurable fronthaul and the BBU pool is capable of performing part of the baseband processing.

The functional split options that can be applied for the vSCs are given in [2]. Considering the potential centralization gains, we have selected the following functional split options as targets in this paper (shown in Fig. 1):

- Standard CRAN – all the baseband processing is done centrally at the BBU pool;
- UpperPHY/LowerPHY – the LowerPHY layer processing is done by the vSC whereas UpperPHY and above is executed by the BBU pool;
- MAC/PHY – the whole PHY layer processing takes place at vSCs whereas MAC and above layers are done at the central BBU pool.

III. System Model

A state vector $\boldsymbol{S}_t = [S_t^1, S_t^2, \ldots, S_t^N]$ represents the possible operative mode of the N vSCs in a cluster at time t . Each single element S_t^i is defined as:

$$\boldsymbol{S}_t^i = \begin{cases} 0, & \text{if } i^{\text{th}} \text{ vSC is switched off} \\ 1, & \text{if } i^{\text{th}} \text{ vSC is in CRAN split mode} \\ 2, & \text{if } i^{\text{th}} \text{ vSC is in UpperPHY/LowerPHY mode} \\ 3, & \text{if } i^{\text{th}} \text{ vSC is in MAC/PHY mode} \end{cases} \tag{1}$$

The energy harvested by each vSC at time t is defined within the state vector $\boldsymbol{E}_t = [E_t^1, E_t^2, \ldots, E_t^N]$, whereas the energy stored by each vSC at time t is defined by the state vector $\boldsymbol{B}_t = [B_t^1, B_t^2, \ldots, B_t^N]$. The traffic load experienced by each vSC is defined by the vector $\boldsymbol{\rho}_t = [\rho_t^1, \rho_t^2, \ldots, \rho_t^N]$.

A. Power model

The power consumption of each split option is estimated based on the model introduced in [10], which is a general flexible power model of LTE base stations and provides the power consumption in Giga Operation Per Second (GOPS). Technology dependent GOPS to Watt conversion factor is applied to determine the power consumption in Watts. In this paper, we have mapped the various baseband processing tasks of the functional split options to their power requirement estimations. The main baseband tasks associated with the split options are shown in Fig. 1.

The total base station power consumption is given by:

$$P_{\text{BS}} = P_{\text{BB}} + P_{\text{RF}} + P_{\text{PA}} + P_{\text{overhead}} \tag{2}$$

where P_{BB} is the power consumption due to baseband processing, P_{RF} is the power consumption due to RF circuitry including transmitter and receiver side, P_{PA} is the power consumption by the power amplifier and P_{overhead} is the overhead power consumption, e.g., cooling system.

The baseband power consumption, P_{BB}, is generally computed as:

$$P_{\text{BB}} = P_{\text{BB1}} + P_{\text{BB2}} \tag{3}$$

More in detail, P_{BB1} is given by:

$$P_{\text{BB1}} = [P_{\text{CPU}} + P_{\text{OFDM}} + P_{\text{filter}}] \tag{4}$$

where P_{CPU} is the idle mode power consumption, P_{OFDM} is the power consumption due to OFDM processes and P_{filter} is the power consumption due to filtering. In addition, P_{BB2}, is given by:

$$P_{\text{BB2}} = [P_{\text{FD}} + P_{\text{FEC}}] \tag{5}$$

where P_{FD} is the frequency domain processing power consumption and P_{FEC} is the power consumption due to FEC processes. Estimating these power consumption values mainly depends on bandwidth, number of antennas and the load fraction. In particular, P_{FD} and P_{FEC} are dependent on the traffic load vector $\boldsymbol{\rho}_t$. The power dependence on these factors can be both linear and exponential [10].

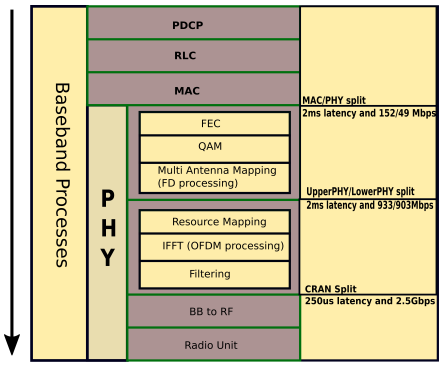

Fig. 1. BBU functions with the considered functional splits and the relevant fronthaul latency and bandwidth requirements (estimated based on [2])

The baseband power consumption of the vSC depends on the adopted functional split option, in particular it is given as:

$$P_{\mathrm{BB}}^{\mathrm{vSC}} = \begin{cases} 0, & \text{if vSC is in CRAN} \\ P_{\mathrm{BB1}}, & \text{if vSC is in UpperPHY/LowerPHY} \\ P_{\mathrm{BB1}} + P_{\mathrm{BB2}}, & \text{if vSC is in MAC/PHY} \end{cases} \tag{6}$$

The power consumption of the MBS is determined by (2). Additional MBS power consumption is considered based on the functional split option of the vSCs in the same mobile cluster (e.g., additional P_{BB2} for each vSC in UpperPHY/LowerPHY split).

IV. Optimal Solution

A. Problem Statement

The intelligent energy management decision is a sequential process that selects the optimal configuration of the N vSCs in the cluster based on the traffic demand, the energy reserve and the future energy arrivals. The objective is to minimize the power drained from the grid which, in turn, is equivalent to MBS power consumption, and avoid system outage. We define system outage as the event to not satisfy the traffic demand due to battery energy depletion or wrong configuration decisions. These wrong configurations may overload the MBS radio access with the traffic of the handed over UEs of the switched off vSCs.

The process evolves in cycles along with the traffic demand and the energy arrival variations. At each cycle t, the task of the centralized controller, which is located at the MBS site, is to select the optimal operative mode of each vSC among the four options given by (1). The minimization of the MBS power consumption is modeled as a DP optimization problem and it is given by:

$$\begin{aligned} &\min_{\{\boldsymbol{S}_t\}_{t=1,\dots,K}} \sum_{t=1}^{K} f(\boldsymbol{S}_t, t) \\ &\text{subject to } B_t^{(i)} > B_{\mathrm{th}} \ \forall i. \end{aligned} \tag{7}$$

where B_{th} is the battery threshold level adopted to prevent damages to the storage devices and K is the time horizon or the number of times the energy control is applied and $f(\boldsymbol{S}_t, t)$ is the cost function at time step t, which is defined as:

$$f(\boldsymbol{S}_t, t) = w_1 \cdot \mathrm{P_m}(\boldsymbol{S}_t, t) + w_2 \cdot \mathrm{D}(\boldsymbol{S}_t, t) \tag{8}$$

where $\mathrm{P_m}(\boldsymbol{S}_t, t)$ and $\mathrm{D}(\boldsymbol{S}_t, t)$ are respectively the grid power consumption and the traffic drop rate of the system, given the operative modes of the vSCs and the time step t. The grid power consumption at time t, $\mathrm{P_m}(\boldsymbol{S}_t, t)$, is equivalent to the power consumption by MBS and is determined based on (2). The traffic drop rate at time t, $\mathrm{D}(\boldsymbol{S}_t, t)$, is the total amount of traffic demand that cannot be served by the system in the time step t, i.e., the sum of the traffic of all the UEs that are not served neither by their vSC, which is switched off, nor by the MBS, which is overloaded. The weights w_1 and w_2 provide flexibility in the cost function to emphasize one part of the cost over the other. They must always sum to 1, that is, $w_1 + w_2 = 1$.

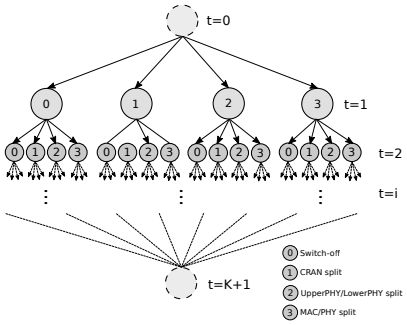

Fig. 2. Graphical representation of the functional split configuration decision process for the case of one vSC

B. Graphical Representation

The problem of finding the optimal operating modes is represented as a graph. In the graph, a single node (N_t^i) represents a possible combination of operating modes of the vSCs. These combinations result in different grid power consumptions, system drop rates and energy storage levels of vSCs. In Fig. 2, an example of graph for a system with a single vSC is depicted. At first time step $(t = 1)$, the vSC can be in one of the four possible operating modes: switch off, CRAN split mode, UpperPHY/LowerPHY split mode and MAC/PHY split mode. Moving one time step ahead, the energy harvesting and traffic demands are also evolving. Hence, each node (N_t^i) generates four possible child nodes corresponding to the four possible operating modes at cycle $t+1$, $(N_{t+1}^j), j = 1, ..., 4$. The number of such possible combinations keeps on evolving until reaching the time horizon K, leading to the maximum number of possible paths at time instant K.

At cycle $t+1$, the battery level corresponding to the child nodes is calculated based on:

$$\boldsymbol{B}_{\mathrm{t+1}} = \min(\boldsymbol{B}_{\mathrm{t}} + \boldsymbol{E}_{\mathrm{t}}, B_{\mathrm{cap}}) - \mathbf{P}_{\mathrm{vSC}}(\mathbf{S}_{\mathrm{t}}) \cdot \Delta_t \tag{9}$$

where B_{cap} is the maximum capacity of the battery in kWh, Δ_t is the time between two consecutive cycles, $\mathbf{P}_{\mathrm{vSC}}(\mathbf{S}_t)$ is a vector representing the power consumption of the vSCs depending on their operative modes. The cost function (8) is used to compute the cost associated to each arc connecting two nodes. Two artificial nodes have been added at time step $t = 0$ and $t = K+1$, to have a single initial node and a single terminal node. The cost associated to the arcs connecting the artificial nodes are set to zero. The cost associated to each arc of the graph can be interpreted as its length. Hence, the optimization problem in (7) is equivalent to finding the shortest path from the initial node at time $t = 0$ to the terminal node at time $t = K + 1$.

C. Shortest Path Search

We consider the Label Correcting Algorithm [11] for finding the shortest path. The exploration of the graph is done in a

depth-first approach by sequentially discovering shorter paths from the starting node to the intermediate nodes until reaching the destination node. We define the variable d_i, called *label of i*, as the length of the shortest path to the node i, OPEN as the list of nodes to be explored and UPPER as the last found minimum-length path. Initially both UPPER and d_i are set to ∞. Throughout the exploration process, the length of the shorter path found so far is maintained in d_i. If a new path is found with shorter length to i, the algorithm considers whether the labels d_j of the child nodes j can be corrected by setting d_j to $d_i + a_{ij}$, where a_{ij} is the $arc(i, j)$. The nodes that are candidates to be included in the shortest path are maintained in the list OPEN. Nodes that result in a path length longer than UPPER or those that cannot satisfy the battery and system constraints are excluded from this candidate list. The steps of the algorithm are shown in Algorithm 1. This exploration policy is relatively faster and requires lower memory by avoiding to explore the whole graph [11]. This is especially advantageous for a tree-like problem such as the one tackled in this work.

Algorithm 1 Shortest Path Search Algorithm

```
initialize OPEN with possible states at time t
while OPEN is not empty do
    remove a node N_t^i
    compute B_{t+1,j}, j = 1, .., 4^N, for all S_{t+1} using (9)
    for each node N_{t+1}^j child of N_t^i do
        a_ij = f(S_{t+1,j}, t + 1)
        if d_i + a_ij < min{d_j, UPPER}
                    and B_{t+1,j} > B_th  then
            d_j ← d_i + a_ij
            set N_t^i parent of N_{t+1}^j
            if t ≠ K then
                place N_{t+1}^j in OPEN (if not already)
            else
                UPPER = d_i + a_ij
            end if
        end if
    end for
end while
```

V. Results and Discussion

A. Simulation Scenario

We consider an area of 1×1 km^2 covered by a MBS with co-located BBU pool placed at the center and connected to the electrical grid. Capacity enhancement is provided by 3 vSCs equipped with a solar panel and a battery. A time horizon of 21 hours (i.e., $K = 21$) is selected, as it represents a reasonable balance between algorithm performance and complexity as described in [9]. User activities are categorized based on [12] as heavy users with an activity of 900 MB/hr and ordinary users with an activity of 112.5 MB/hr. Moreover, we adopt the traffic profiles described in [13], in particular the residential and office ones. The solar energy traces are generated using the SolarStat tool [14] for the city of Los Angeles and simulations are carried out for the months of January and July, representing the worst and the best energy harvesting month, respectively.

The reference vSC power consumption values for our scenario are $P_{\mathrm{RF}} = 2.6$ W and $P_{\mathrm{PA}} = 71.4$ W. For P_{BB}, we consider 200 GOPS, 160 GOPS and 80 GOPS for P_{CPU}, P_{filter} and P_{OFDM} respectively. Moreover, the reference load dependent power consumption values are 30 GOPS, 10 GOPS and 20 GOPS for linear component of P_{FD}, non-linear component of P_{FD} and P_{FEC} respectively. As for the MBS, we consider $P_{\mathrm{RF}} = 9.18$ W and $P_{\mathrm{PA}} = 1100$ W. The baseband power consumption is 630 GOPS and 215 GOPS for the static ($P_{\mathrm{CPU}} + P_{\mathrm{OFDM}} + P_{\mathrm{filter}}$) and load dependent components ($P_{\mathrm{FD}} + P_{\mathrm{FEC}}$), respectively. The power consumption overhead (P_{overhead}) is of 0 and 10% of the total power of the rest of the base station for the case of vSC and MBS, respectively. Other simulation parameters are given in Table I.

TABLE I
Simulation Parameters.

Parameter	Value
Solar panel size (m^2)	4.48
Solar panel efficiency (%)	20
Transmission power of macro cell (dBm)	43
Transmission power of vSC (dBm)	38
Bandwidth (MHz)	5
Antenna	2x2
Battery capacity (kWh)	2
Battery threshold (%)	20
GOPS to Watt conversion factor	8
w_1, w_2	0.5

B. Optimal Functional Split Configurations

The result of optimal functional split placement decisions for a scenario involving 3 vSCs with 90 users per vSC in a residential area is shown in Fig. 3. Heavy users ratio of 50% is considered. The policy is able to decide the placement of the baseband functions in accordance with the available energy, forecasted harvested energy and traffic demands. Hence the result shows that, most of the user traffic is handled by the vSCs with no outage. Moreover, for a January week, the CRAN and MAC/PHY are the most chosen split options during daytime and peak traffic periods whereas switching off occurs during very low traffic hours. The average CRAN and MAC/PHY selection rate is 37% each and switching off rate is averaged at 20%. The results of the simulation for a week of July shows that MAC/PHY split mode is the most selected option. Average MAC/PHY selection rate is 67%, whereas switching off rate is averaged at 8%. This confirms that due to high energy availability, the vSCs are performing most of the baseband processes by themselves which, in turn, further reduces the grid energy consumed by the MBS.

The result of optimal functional split placement for a scenario of 3 vSCs deployed in an office area with 90 users per vSC is shown in Fig. 4. Heavy users ratio of 50% is considered. An office area traffic profile is characterized by relatively lower traffic peak both in weekdays and weekends. In addition, the peak traffic hours are different than the residential traffic profile

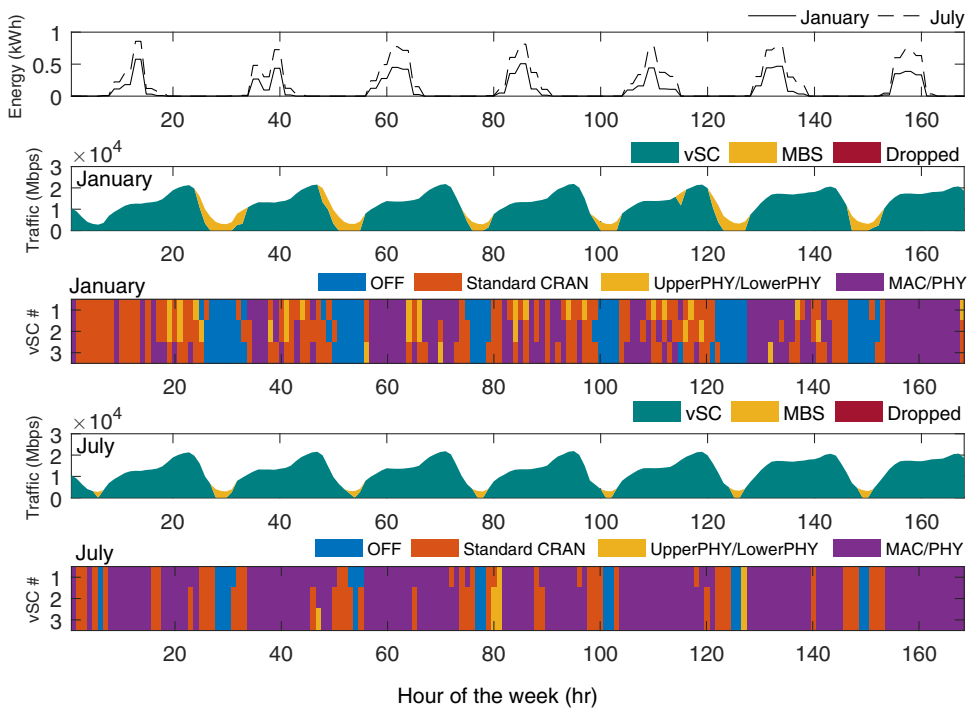

Fig. 3. Optimal functional split placement results in a residential area scenario for a week of January and July (hour 0 to hour 168; Monday from 0 - 23 hr). The traces show the amount of harvested energy, the amount of mobile traffic handled by vSCs and MBS and operative mode of each vSCs for both January and July weeks.

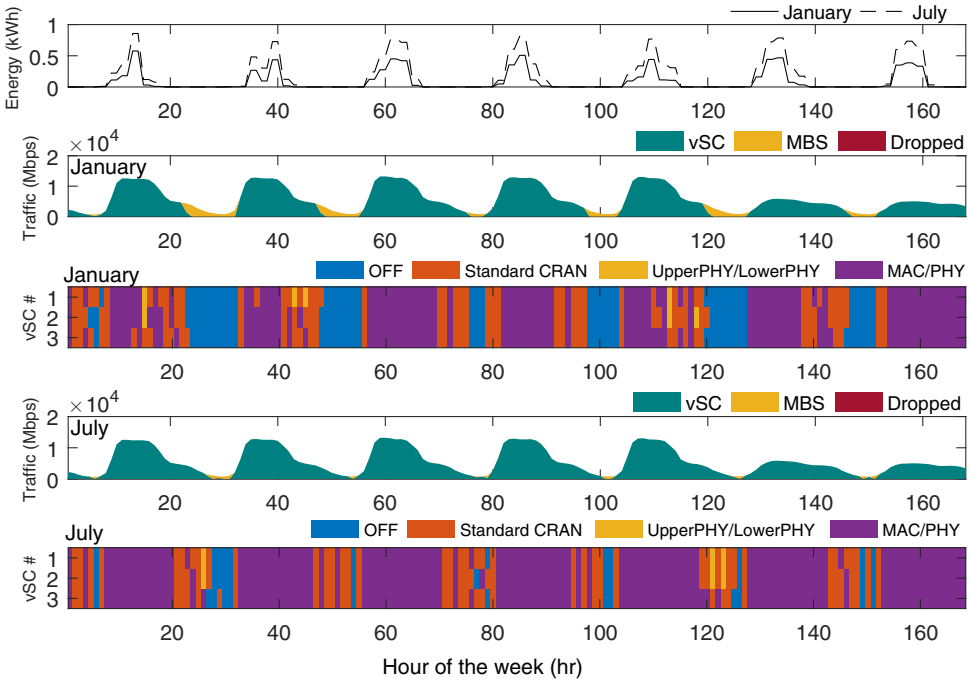

Fig. 4. Optimal functional split placement results in an office area scenario for a week of January and July (hour 0 to hour 168; Monday from 0 - 23 hr). The traces show the amount of harvested energy, the amount of mobile traffic handled by vSCs and MBS and operative mode of each vSCs for both January and July weeks.

and more aligned with the solar energy arrivals. The result shows that the dynamic placement of the baseband functions enable the vSCs to offload the MBS for most of the users traffic without any drop. In addition, MAC/PHY and CRAN operative modes are the most selected options in January during peak traffic periods. The average MAC/PHY and CRAN selection rate is 47% and 28% respectively. Average switch off rate is at 23% and occurs during very low traffic periods, i.e. during night. In July, MAC/PHY is the most selected operative mode with an average selection rate of 68% and occurring during peak traffic periods, whereas, switch off occurs during very low traffic hours with average rate of 7.3%. This is due to the higher energy income in July. The high selection rate of MAC/PHY split results in a further reduction of grid energy consumption, since most of the baseband processes are performed locally by vSCs.

C. Comparison with static policies

This subsection provides a comparative analysis of the proposed optimal solution with static functional split policies. In the static solutions, the vSCs are kept in the same split mode as long as the battery level is above the threshold, otherwise it is switched off. The results of these static policies for a scenario with 3 vSCs deployed in a residential area with 90 users each and a heavy user ratio of 50% for a week of January and July are shown in Table II. All the static policies are not capable to reach the traffic drop rate performance of the optimal bound. Moreover, the performance gap can vary importantly with respect to the policy. In fact, the CRAN policy shows smaller outage against both UpperPHY/LowerPHY and MAC/PHY policies. This is mainly due to the low energy consumption of the vSCs in CRAN mode since they do not perform any baseband operation. Both UpperPHY/LowerPHY and MAC/PHY polices experience high drop rates for the case of January. The static policies are also sub-optimal in terms of grid energy consumption, where savings of up to 24 KWh and 29 KWh can be achieved in January and July, respectively.

TABLE II
POLICY COMPARISONS

Policy	Grid energy consumption (KWh)		Average drop rate (%)	
	January	July	January	July
Optimal	149.51	133.23	0	0
CRAN	170.01	162.48	2.35	1.5
UpperPHY/LowerPHY	173.76	153.64	16.43	5
MAC/PHY	173.56	151.40	17.10	5

VI. CONCLUSIONS

In this paper, we have proposed an optimal functional split placement of energy harvesting virtual small cells that relies on central BBU pool for part of their baseband processing. In particular, three functional split options namely, CRAN, UpperPHY/LowerPHY and MAC/PHY, have been targeted. A grid energy consumption minimization problem is stated and Dynamic Programming, more specifically Shortest Path search algorithm, is applied to determine the optimal functional split configurations. Simulation results show that dynamic functional split options placement with optimal control serves the traffic demand with significant energy saving, and hence lower OPEX, with respect to static functional split policies. Therefore, the obtained performance bounds represent an encouraging starting point for the evaluation of more sophisticated online optimization techniques.

ACKNOWLEDGEMENT

This work has received funding from the European Union's Horizon 2020 research and innovation programme under the Marie Sklodowska-Curie grant agreement No 675891 (SCAVENGE) and by Spanish MINECO grant TEC2017-88373-R (5G-REFINE).

REFERENCES

[1] "C-RAN: the road towards green RAN," *China Mobile Research Institute, White Paper*, 2011.

[2] "Virtualization for small cells: overview," *Small cell forum*, 2015.

[3] M. Peng, Y. Li, J. Jiang, J. Li, and C. Wang, "Heterogeneous cloud radio access networks: A new perspective for enhancing spectral and energy efficiencies," *IEEE Wireless Communications*, vol. 21, no. 6, pp. 126–135, 2014.

[4] H. Hawilo, A. Shami, M. Mirahmadi, and R. Asal, "Nfv: state of the art, challenges, and implementation in next generation mobile networks (vepc)," *IEEE Network*, vol. 28, no. 6, pp. 18–26, Nov 2014.

[5] G. Piro, M. Miozzo, G. Forte, N. Baldo, L. A. Grieco, G. Boggia, and P. Dini, "Hetnets powered by renewable energy sources: Sustainable next-generation cellular networks," *IEEE Internet Computing*, vol. 17, no. 1, pp. 32–39, 2013.

[6] G. Lee, W. Saad, M. Bennis, A. Mehbodniya, and F. Adachi, "Online ski rental for ON/OFF scheduling of energy harvesting base stations," *IEEE Transactions on Wireless Communications*, vol. 16, no. 5, pp. 2976–2990, 2017.

[7] M. Miozzo, L. Giupponi, M. Rossi, and P. Dini, "Distributed Q-learning for energy harvesting heterogeneous networks," in *2015 IEEE International Conference on Communication Workshop (ICCW)*, June 2015, pp. 2006–2011.

[8] H. Ameur, M. Esseghir, and L. Khoukhi, "Fully Distributed Approach for Energy Saving in Heterogeneous Networks," in *2016 8th IFIP International Conference on New Technologies, Mobility and Security (NTMS)*, Nov 2016, pp. 1–6.

[9] N. Piovesan and P. Dini, "Optimal direct load control of renewable powered small cells: A shortest path approach," *Internet Technology Letters*, 2017.

[10] C. Desset, B. Debaillie, V. Giannini, A. Fehske, G. Auer, H. Holtkamp, W. Wajda, D. Sabella, F. Richter, M. J. Gonzalez, H. Klessig, I. Godor, M. Olsson, M. A. Imran, A. Ambrosy, and O. Blume, "Flexible power modeling of LTE base stations," in *2012 IEEE Wireless Communications and Networking Conference (WCNC)*, April 2012, pp. 2858–2862.

[11] D. P. Bertsekas, D. P. Bertsekas, D. P. Bertsekas, and D. P. Bertsekas, *Dynamic programming and optimal control*. Athena scientific Belmont, MA, 1995, vol. 1, no. 2.

[12] G. Auer, O. Blume, V. Giannini, I. Godor, M. Imran, Y. Jading, E. Katranaras, M. Olsson, D. Sabella, P. Skillermark *et al.*, "D2. 3: Energy efficiency analysis of the reference systems, areas of improvements and target breakdown," *EARTH*, vol. 20, no. 10, 2010.

[13] F. Xu, Y. Li, H. Wang, P. Zhang, and D. Jin, "Understanding mobile traffic patterns of large scale cellular towers in urban environment," *IEEE/ACM Transactions on Networking (TON)*, vol. 25, no. 2, pp. 1147–1161, 2017.

[14] M. Miozzo, D. Zordan, P. Dini, and M. Rossi, "SolarStat: Modeling photovoltaic sources through stochastic markov processes," in *2014 IEEE International Energy Conference (ENERGYCON)*, May 2014, pp. 688–695.